

Dynamic Characteristic Analysis of a Rotor System with Rub-impact Fault Considering Rotor-stator Misalignment

Abstract. In this paper, taking a single span flexible rotor system with two discs as the research object, the finite element model of the rotor-bearing system is established. The stator is simplified as a group of equispaced points along the circumference and the rotor as a point based on the contact dynamic theory. The rotor-stator rubbing is simulated using multiple point-point contact elements, the separation and the contact of the rotor and stator are determined by the change of the cylindrical gap, and the rotor and stator model are coupled by nonlinear contact force. By adopting the augmented Lagrangian method to deal with contact constraint conditions, Coulomb friction model to simulate rotor-stator frictional characteristics, the responses of the rotor system with rubbing are analyzed. The effects of rotating speeds and rubbing stiffness on normal rubbing forces are discussed under asymmetrical rotor-stator clearance conditions. The results show that there may be different rubbing forms (local rubbing and full rubbing) and transient impact forces under four cases with rotating speeds. Rubbing stiffness has the greatest effects on the rubbing force, the amount of misalignment affects mainly the transient impact force and does not affect the normal rubbing force at the stable rubbing stage.

Streszczenie. Analizowano układ wirnika z dwoma dyskami. Symulowano tarcie między wirnikiem i stojanem a separacja była uwzględniana jako zmiana cylindrycznej szczeliny. (Analiza właściwości dynamicznych systemu z wirnikiem przy uwzględnieniu niewspółosiowości wirnika i stojana)

Keywords. Rubbing, Flexible Rotor System, Finite Element Method, Contact Dynamic, Misalignment

Słowa kluczowe: wirnik, stojan, układ wirujący

Introduction

Due to the increasing demand for a high speed and high efficiency of rotor system, the rotor-stator clearance in modern rotating machinery is becoming smaller and smaller. As a result, the rub-impact, which refers to the contact between the rotating and non-rotating structures in a machine, has become one of the most common damaging malfunctions of rotating machinery [1]. Further investigation on the mechanism of the rub-impact phenomenon and its fault features is integral to the improvement of the current rubbing fault diagnosis.

For the simple rotor system, much research on complicated nonlinear dynamic characteristics caused by rotor-stator rubbing has been undertaken [2]. With the development of the finite element (FE), many researchers employed the FE method to establish the rotor model [3]. The FE method is suitable to simulate the complex structures. In recent years, rotor-stator rubbing simulated by combining the FE method with the nonlinear contact theory has become widely researched. In the governing equations, the dynamics of the rotor and stator are coupled through contact forces. Available approaches in contact mechanics are usually the penalty method, the Lagrange multiplier method and the augmented Lagrangian method [4-9]. At present, there is insufficient research on the interface contact characteristics of rotor-stator rubbing, and it is an area that warrants further investigation [10, 11].

In the rotor system in practice, the geometric centers of the rotor and the stator don't totally coincide due to gravity, assembling and other reasons, namely, that the rotor-stator clearance is not generally uniform. Aiming at this actual situation, in this paper a single span flexible rotor system with two discs is taken as the research object, and the finite element model of the rotor-bearing system is established. The stator is simplified as a group of equispaced points along the circumference and the rotor as a point based on the contact dynamic theory. The rotor-stator rubbing is simulated using multiple point-point contact elements, the separation and contact of rotor and stator are determined by the change of cylindrical gap, and the rotor and stator model are coupled by nonlinear contact force. By adopting the augmented Lagrangian method to deal with contact constraint conditions, the coulomb friction model to simulate rotor-stator frictional characteristics, the responses of the rotor system with rubbing are solved using the Newmark- β

direct integral method combined with Newton-Rapson iteration. The effects of rotating speeds, rubbing stiffness, rubbing damping and friction efficient on normal rubbing forces are discussed under asymmetrical rotor-stator clearance conditions.

Finite element model of a rotor system with rub-impact considering rotor-stator misalignment

Assuming that rub-impact occurs between the disc and the stator, and the stator is fixed, as is shown in Fig. 2. In the figure, o_w is the whirl rotation center, o_r is the geometric center of the rotor, and o_s is the geometric center of the stator. The misalignment position is assumed along z direction and δ denotes the misalignment degree. The rotor is assumed as a point and the stator as a group of points along the circumference direction. The master body is set as the rotor and the slave one is the stator. In view of the contact computation demanding much more time, the stator is divided as 72 nodes for the convenience of analysis, namely, a node is established every five degrees along the circumference direction. Assume that the cross-section of the disc remains in the $y o_w z$ plane. Point c of the disc and point d of the stator are selected as a contact pair shown in Fig. 1, so the gap function g is equal to the distance \overline{cd} .

$$(1) \quad \overline{cd} = \overline{o_w d} - \overline{o_w c}$$

The augmented Lagrangian method is adopted to satisfy the contact condition in this paper. The method properly defines force normal to the contact surface to make the penetration limited to a specific tolerance. Such force is as follows:

$$(2) \quad F_N = \begin{cases} 0 & \text{if } g > 0 \\ k_N g + \lambda_N^{(i+1)} & \text{if } g \leq 0 \end{cases},$$

where k_N is the normal rubbing stiffness, i.e., the penalty factor; g is the transient gap between the rotor and the stator, i.e., penetration; $\lambda_N^{(i+1)}$ is the Lagrange multiplier for $(i+1)$ th iteration, which can be found by

$$(3) \quad \lambda_N^{(i+1)} = \begin{cases} \lambda_N^{(i)} + k_N g & \text{if } |g| \geq \varepsilon \\ \lambda_N^{(i)} & \text{if } |g| < \varepsilon \end{cases},$$

where ε is the specific penetration tolerance. After specific iteration, if the penetration is still greater than ε , the contact stiffness/rubbing stiffness of the contact element will be augmented through the Lagrange multiplier. This procedure is repeated until the penetration is less than ε .

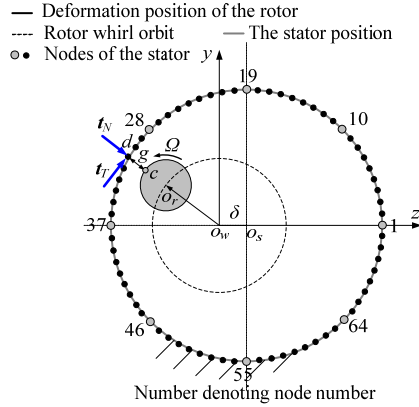


Fig. 1. Rub-impact model considering rotor-stator misalignment

Considering fixed-point rubbing and external force action, the equation of motion of a rotor-bearing system can be written as follows:

$$(4) \quad \begin{bmatrix} \mathbf{M} & \mathbf{0} \\ \mathbf{0} & \mathbf{0} \end{bmatrix} \ddot{\mathbf{u}} + \begin{bmatrix} \mathbf{G} + \mathbf{C} & \mathbf{0} \\ \mathbf{0} & \mathbf{0} \end{bmatrix} \dot{\mathbf{u}} + \begin{bmatrix} \mathbf{K} + k_N \mathbf{B}^T \mathbf{B} & \mathbf{B}^T \\ \mathbf{B}^T & \mathbf{0} \end{bmatrix} \begin{bmatrix} \mathbf{u} \\ \boldsymbol{\lambda} \end{bmatrix} = \begin{bmatrix} \mathbf{F}_u - k_N \mathbf{B}^T D_0 \\ -D_0 \end{bmatrix}$$

where \mathbf{M} , \mathbf{G} , \mathbf{C} , \mathbf{K} and \mathbf{u} respectively denote mass, gyroscopic, damping (including bearing and viscous damping) and stiffness (including rotor and bearing stiffness) matrixes and displacement vector of the global system; $\boldsymbol{\lambda}$ is a vector related to Lagrange multiplier; \mathbf{B} is the contact constraint matrix in the normal and tangential directions; D_0 is the initial normal gap and \mathbf{F}_u is the external load vector.

Numerical simulation

The schematic diagram of the rotor-bearing system with rub-impact is shown in Fig. 2. The simulation parameters are as follows: elastic modulus $E = 2.07 \times 10^{11}$ Pa, Poisson's ratio $\nu = 0.3$, material density $\rho = 7850$ kg/m³. Assuming that two discs are identical, namely, there are the same unbalances for two discs, the unbalance is set as $m.r = 1.56 \times 10^{-4}$ kg·m. For the left bearing, the horizontal stiffness and damping are $k_{zl} = 1 \times 10^5$ N/m, $c_{zl} = 2 \times 10^3$ N·s/m respectively, the vertical stiffness and damping $k_{yl} = 2 \times 10^5$ N/m, $c_{yl} = 2 \times 10^3$ N·s/m. For the right bearing, the horizontal stiffness and damping are $k_{zr} = 2 \times 10^8$ N/m, $c_{zr} = 2 \times 10^5$ N·s/m respectively, the vertical stiffness and damping $k_{yr} = 5 \times 10^8$ N/m, $c_{yr} = 2 \times 10^5$ N·s/m.

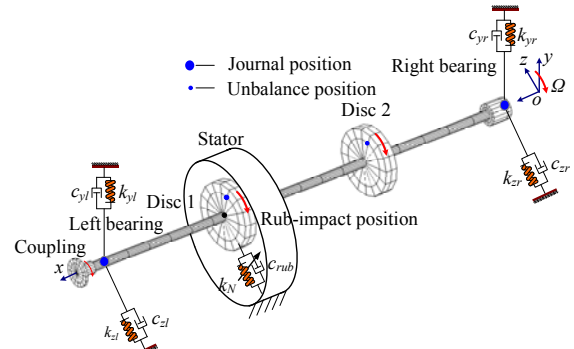


Fig. 2. Schematic diagram of the rotor-bearing system with rub-impact

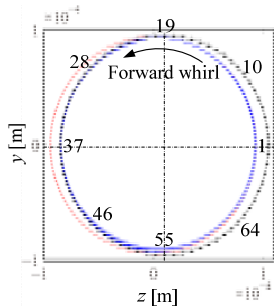
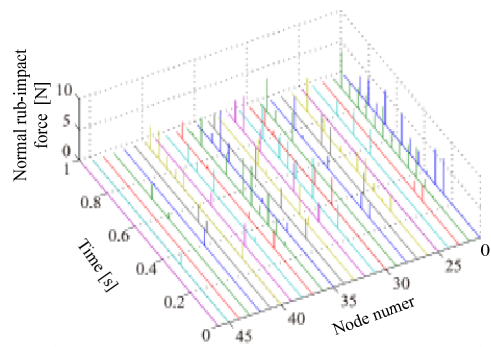
The first and second critical speeds can be determined as 1667 and 6420 r/min based on above parameters. Assume that the rub-impact occurs between the disc 1 and its corresponding stator, and the stator is fixed. In the next sections, the effects of rotating speeds, misalignment clearances and rubbing stiffnesses on normal rubbing forces are discussed under asymmetrical rotor-stator clearance conditions.

The effects of rotating speeds

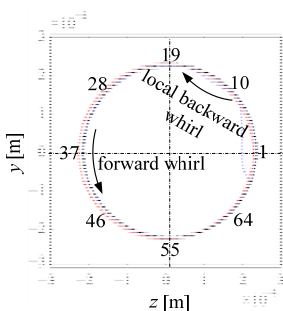
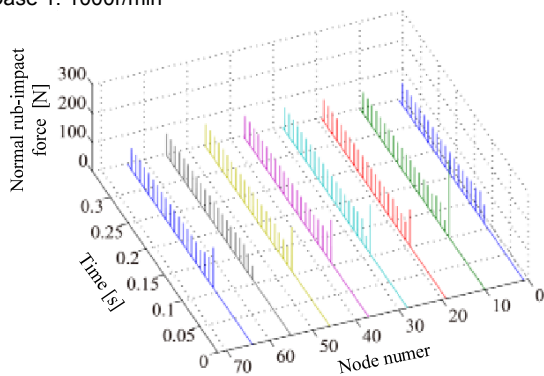
To describe the effect of rotating speeds, four rotating conditions 1000, 5000, 8500 and 10000 r/min are selected in this study. Rub-impact stiffness (rotor-stator normal contact stiffness) is assumed as $k_N = 8 \times 10^7$ N/m, friction efficient $\mu_f = 0.3$ without regard to rub-impact damping.

To simulated rub-impact behavior under different conditions, the clearance between the rotor and the stator is assumed as 95, 225, 220 and 220 μm for the above mentioned four conditions, the corresponding misalignments are all $\delta = 10 \mu\text{m}$. The simulation results are shown in Fig. 3, for the normal rub-impact force, the ordinate is the normal rub-impact force with unit Newton (N), the abscissa of left side is time with unit second(s) and the abscissa of right side is node number. For the rotor orbit, the abscissa is the horizontal displacement with unit meter (m) and the ordinate is the vertical displacement with unit meter (m); in the figure, the red line and the blue line denote the rotor trajectory before and after the rub-impact occurs, respectively, and the black line denotes the rotor-stator circular clearance. The direction of arrow shows the direction of the rotor whirl and the direction of rotation is counterclockwise.

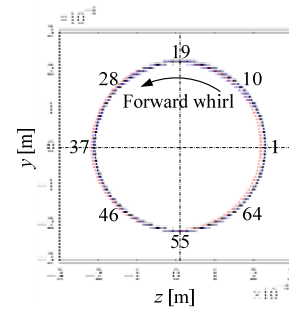
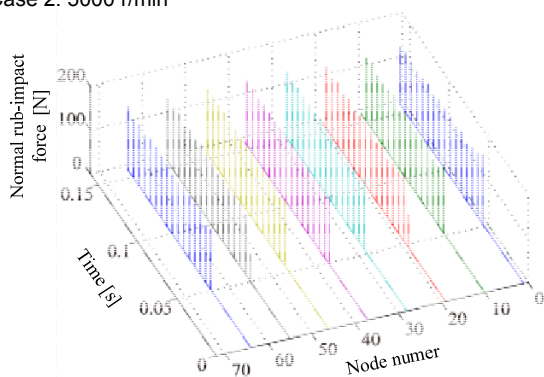
The simulation result is shown in Fig. 3(a) under condition 1. From the rotor orbit, it can be seen that the local rub-impact occurs. The normal rub-impact force only exists between element 21 and element 46, the collision involving the nodes 21, 22 and 30-36 is relatively serious and slight for other nodes. The normal rub-impact force for nodes 21 and 36 is shown in Fig. 5. From the figure, it can be seen that the collision time interval is uniform and the amplitude of the force is different before 0.6s, which shows that the each collision degree is different but that the collision position is same. The collision times of node 36 decreases in contrast with that of node 21 after 0.6s. From the rotor orbit, it can be seen that the rub-impact mainly appears on the left side due to the asymmetry clearance and does not on the right side, so this contact condition belongs to local rubbing. In this condition, the direction of whirl is the same as that of rotation and forward whirl.



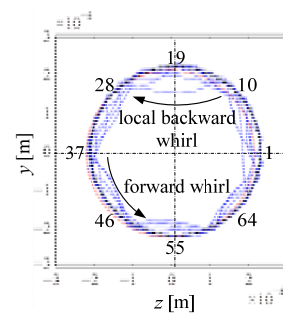
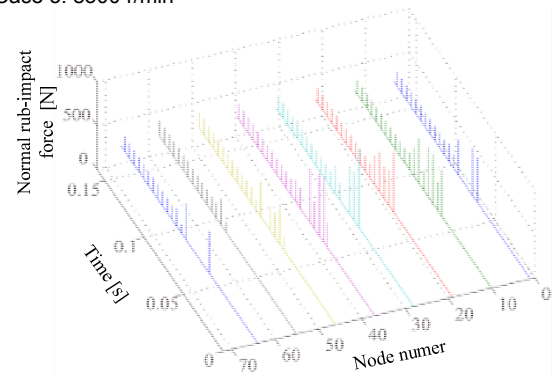
(a) Case 1: 1000r/min



(b) Case 2: 5000 r/min



(c) Case 3: 8500 r/min



(d) Case 4: 10000 r/min

Fig. 3. Normal rub-impact force and rotor orbit when $\delta = 10 \mu\text{m}$

With the increase of the rotating speed, the full rubbing occurs under the cases 2, 3 and 4. The rotor slides along the stator surface after the rotor motion is stable. In order to draw clear, only normal rub-impact forces of eight contact points of 1, 10, 19, 28, 37, 46, 55 and 64 are plotted, as are shown in Fig. 3(b), 3(c) and 3(d). The normal contact force is greater and about 269 N at node 10 when the initial rub-impact appears under the case 2. The rub-impact is stable and the normal contact force about 74 N after the rebounds are sustained four times. The local backward whirl appears at the initial rebound stage, but the whole whirl direction is forward, as is arrowed in Fig. 3(b). Under the case 3, the rotor orbit is stable and coincides with the stator boundary even at the initial rebound stage and the normal rub-impact force is also stable and about 145 N, as is shown in Fig. 4(c). Under the case 4, the initial impact is greater than these of cases 2 and 3, and is about 900 N at node 28 and sustains about six periods before the stable rub-impact appears. The collision rebound is larger at the initial rub-impact stage, which contributes to the local rub-impact, and become weaker at the stable rub-impact stage which contributes to the full rub-impact. The whirl form is similar to case 2, as is arrowed in Fig. 3(d).

Taking nodes 28 and 37 as example, the initial and stable rub-impact force, and the time interval of the two rub-impacts is analyzed, as is shown in Table 1. From the table,

it can be seen that the stable rub-impact force increases with the increase of the rotating speed. Local rub-impact appears and rub-impact is unstable and fluctuates greatly under case 1. From the rub-impact time, it can be seen that unstable rub-impact period appears at node 28, namely, there is one rub-impact every one period (time interval 0.06 s), four periods and six periods, respectively. However there is one rub-impact every one period, two periods, three periods and five periods at node 37, respectively. Under

case 2, the initial rub-impact force is greater and about two times that of the stable rub-impact force. However under case 3, the initial impact is close to that at the steady-state. The initial impact force is about five times that of the stable rub-impact force and continues for a long time under case 4. For the 72 nodes, one rub-impact appears every revolution, namely full rub-impact occurs. The features of rub-impact for nodes 28 and 37 are listed in Table 1.

Table 1. Feature comparison of normal rub-impact forces under four cases

Cases (r/min)	Node	Initial normal rub-impact force (N)	Stable normal rub-impact force (N)	Time interval of rub-impact (s)
1000	28	2.4	0.5~5.3	0.06,0.24,0.36
	37	3	0.5~5.3	0.06,0.12,0.18,0.3
5000	28	170	79	0.012
	37	148	79	0.012
8500	28	163	143~150	0.0071
	37	157	143~153	0.0071
10000	28	900	175	0.006
	37	758	179	0.006

The effects of misalignment clearances and rub-impact stiffnesses

From the analysis at above section, it is clear that rub-impact condition is the most complicated under case 4 condition. So in the following, misalignment clearances, and rub-impact stiffnesses on the effects of the rub-impact force are analyzed. The simulation parameters and results are shown in Table 2 and Figs 3-5, respectively. In the Figs 4,5, the coordinate axes are the same as these in Fig. 4.

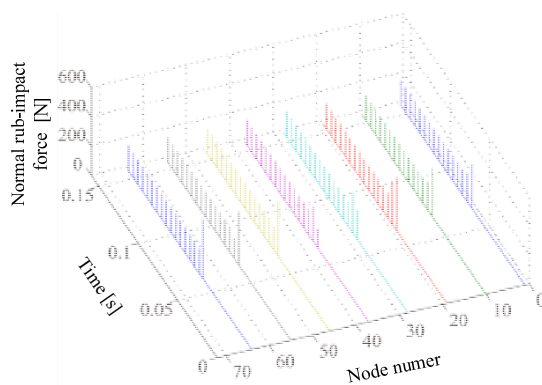
The normal rub-impact force of eight contact nodes considering misalignment clearances of $\delta = 5, 10, 15$ mm are shown in Figs. 4(a), 3(d) and 4(b). From the figures, it can be observed that rub-impact is stable and the rub-impact forces are all closed to 180 N during the steady-state rub-impact stage. However the initial rub-impact force changes greatly, the maximum value is about 406 N and the time interval from unstable to stable rub-impact about two periods when $\delta = 5$ mm, about 900 N and seven periods

when $\delta = 10$ mm, about 740 N and five periods when $\delta = 15$ mm.

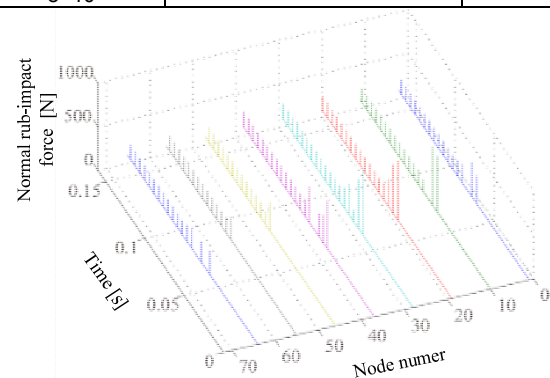
Normal rub-impact force of eight contact nodes considering rub-impact stiffnesses of $k_N = 8 \times 10^7, 8 \times 10^6, 8 \times 10^5$ N/m are shown in Figs. 3(d), 5(a) and 5(b). From the figures, it can be observed that rub-impact force changes greatly, the initial rub-impact force is about 900 N and stable rub-impact about 180 N when $k_N = 8 \times 10^7$ N/m. The initial rub-impact decrease greatly the minimum is about 32 N, which is less than the stable rub-impact force 80 N when the rub-impact stiffness reduces to $k_N = 8 \times 10^6$ N/m. The rub-impact of contact nodes is irregular and the largest rub-impact force is less than 6 N, here the rub-impact is local when $k_N = 8 \times 10^5$ N/m.

Table 2. Numerical simulation parameters

Control parameter	Figures	δ (mm)	k_N (N/m)	c_{rub} (N.s/m)	μ_f
Asymmetrical clearance (δ)	Fig. 4(a)	5	8×10^7	0	0.3
	Fig. 3(d)	10			
	Fig. 4(b)	15			
Rub-impact stiffness	Fig. 3(d)	10	8×10^7	0	0.3
	Fig. 5(a)		8×10^6		
	Fig. 5(b)		8×10^5		

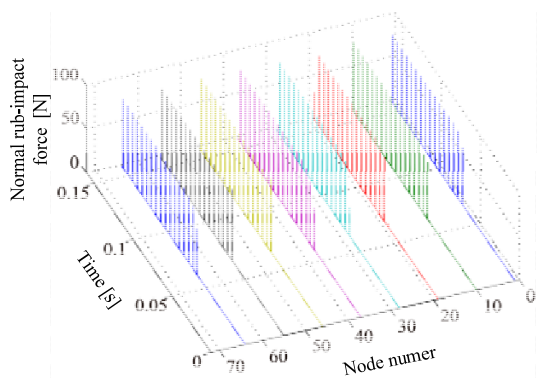


(a) $\delta = 5$ mm

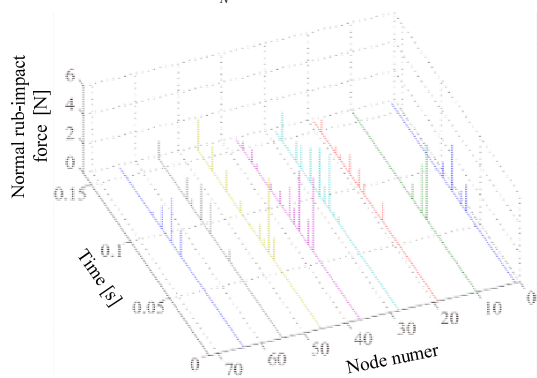


(b) $\delta = 15$ mm

Fig. 4. The effects on normal rub-impact force at different δ



(a) $k_N = 8 \times 10^6$ N/m



(b) $k_N = 8 \times 10^5$ N/m

Fig. 5. The effects on normal rub-impact force at different rub-impact stiffnesses

Conclusions

In this paper, the finite element model of the rotor-bearing system is established and multiple point-point contact elements are used to simulate the rotor-stator rub-impact fault due to asymmetrical clearance, some conclusions are obtained as follows:

1) Normal rub-impact force increases with the increase of the rotating speed. The rub-impact force is small due to weak bounce at small rotating speed (1000 r/min), here the rub-impact is partial and the collision degree is different for the participant nodes. The full rub-impact occurs after larger initial impact appears at other rotating speeds (5000, 8500 and 10000 r/min), the impact time continues for a long time and the transient impact force is greater than stable rub-impact force.

2) The rub-impact stiffness has great influence on the normal rub-impact force, especially on the initial renounce. Rotor-stator asymmetrical clearance has some influence on the normal rub-impact force at initial rub-impact stage, and less influence on the stable normal rub-impact force.

Acknowledgments

We are grateful to the China Natural Science Funds (NSFC, Grant No. 50805019) and the Fundamental Research Funds for the Central Universities (Grant No. N100403008).

REFERENCES

- [1] Muszynska A., Rotordynamics, CRC Press, Boca Raton (2005)
- [2] Ehrich F., High-order subharmonic response of high-speed rotors in bearing clearance, Journal of Vibration Acoustics Stress and Reliability in Design-Transactions of the ASME, 110 (1988), 9-16
- [3] Nelson H. and Mcvaugh J., The dynamics of rotor-bearing systems using finite elements, ASME Journal of Engineering for Industry, 98 (1976), No. 2, 593-600
- [4] Belytschko T., Liu W. K. and Moran B., Nonlinear Finite elements for continua and structures, John Wiley & Sons Ltd, New York (2000).
- [5] J. C. Simo and T. A. Laursen, Computers and structures 42, 97 (1992).
- [6] Laursen T. A., Computational Contact and Impact Mechanics: Fundamentals of Modeling Interfacial Phenomena in Nonlinear Finite Element Analysis, Springer, Berlin (2003).
- [7] Wriggers P., Computational Contact Mechanics, Wiley, New York (2002).
- [8] Qin F., Chen L. M., Y. Li and Zhang X. F., Fundamental frequencies of turbine blades with geometry mismatch in fir-tree attachments, ASME Journal of Turbomachinery, 128 (2006), 512-516.
- [9] Xu D. Q., A new node-to-node approach to contact/impact problems for two dimensional elastic solids subject to finite deformation. PhD Thesis, The University of Illinois at Urbana-Champaign, (2008).
- [10] Chen S., Geradin M., Finite element simulation of non-linear transient response due to rotor-stator contact, Engineering Computations, 14 (1997), No. 6, 591-603
- [11] S. Roques, M. Legrand, P. Cartraud, C. Stoisser and C. Pierre, Modeling of a rotor speed transient response with radial rubbing, Journal of Sound and Vibration, 329 (2010), 527-546

Authors

Authors: Dr. Hui Ma, Department of Mechanical Engineering & Automation, Northeastern University, Shenyang, Liaoning 110819, P R China. E-mail: mahui_2007@163.com.